

Asymmetry in earthquake interevent time intervals

Yongwen Zhang^{1,2,3}, Yosef Ashkenazy² & Shlomo Havlin³

¹Data Science Research Center, Faculty of Science, Kunming University of Science and Technology,
Kunming 650500, Yunnan, China,

²Department of Solar Energy and Environmental Physics, The Jacob Blaustein Institutes for Desert
Research, Ben-Gurion University of the Negev, Midreshet Ben-Gurion 84990, Israel,

³Department of Physics, Bar-Ilan University, Ramat Gan 52900, Israel

Key Points:

- We study the asymmetry of earthquake interevent time intervals which exhibits a crossover.
- We suggest that the mechanism of the observed asymmetry is related to the earthquake triggering processes.
- The observed asymmetry is better reproduced by an improved ETAS model developed recently.

arXiv:2108.06137v1 [physics.geo-ph] 13 Aug 2021

Abstract

Here we focus on a basic statistical measure of earthquake catalogs that has not been studied before, the asymmetry of interevent time series (e.g., reflecting the tendency to have more aftershocks than spontaneous earthquakes). We define the asymmetry metric as the ratio between the number of positive interevent time increments minus negative increments and the total (positive plus negative) number of increments. Such asymmetry commonly exists in time series data for non-linear geophysical systems like river flow which decays slowly and increases rapidly. We find that earthquake interevent time series are significantly asymmetric, where the asymmetry function exhibits a significant crossover to weak asymmetry at large lag-index. We suggest that the Omori law can be associated with the large asymmetry at short time intervals below the crossover whereas overlapping aftershock sequences and the spontaneous events can be associated with a fast decay of asymmetry above the crossover. We show that the asymmetry is better reproduced by a recently modified ETAS model with two triggering processes in comparison to the standard ETAS model which only has one.

Plain Language Summary

Earthquakes are often associated with non-equilibrium and nonlinear underlying processes which can lead to asymmetric behavior in metrics derived from earthquake records. By asymmetry we are referring to ‘the tendency of more events to occur after a previous one than before the next one’ or vice versa. In earthquake sequences the main source of asymmetry is the occurrence of large numbers of aftershocks due to the earthquake triggering. We find here that the distributions of interevent time increments in real seismic catalogs are asymmetric and that the degree of asymmetry is characterized by a scaling function that exhibits a crossover, from a high asymmetry at short times to low asymmetry at long times. We suggest that different earthquake triggering processes are associated with these two distinct regimes of asymmetry. We apply the asymmetry analysis to an earthquake forecasting model—the Epidemic–Type Aftershock Sequence (ETAS) model and find that the new generalized ETAS model that includes both short- and long-term triggering mechanisms better reproduces the observed asymmetry than the standard ETAS model.

1 Introduction

Earthquakes are a major threat to society in many countries around the world. Currently, a skillful and trustworthy earthquake forecasting approach for both short and long time scales is missing. Yet, it is necessary to establish reasonable reduction strategies of seismic risk and enhance alertness and resilience. In most cases, seismologists are not yet able to predict individual large earthquakes even very close to the event (Jordan et al., 2011; de Arcangelis et al., 2016).

Earthquake catalogs are usually restricted to specific regions and include the magnitude, location, and time of earthquakes. Several seismic laws have been discovered based on earthquake records. According to the Gutenberg-Richter law, the number of earthquakes N (above a magnitude M) drops exponentially with the magnitude such that, $\log_{10} N = a - bM$, where $b \approx 1$ and a is related to the earthquake rate (Gutenberg & Richter, 1944). Most earthquakes are distributed along active seismic faults which can be clearly seen in the global catalog (Ide, 2013). In addition, aftershocks occur around the epicenter of the mainshock and the distribution of distances from the mainshock follows a power law decay (Ogata, 1988; Huc & Main, 2003; Marsan & Lengliné, 2008), which is related to the static or dynamic stress triggering mechanism (Richards-Dinger et al., 2010; Lippiello et al., 2009).

63 The temporal occurrence of spontaneous earthquakes (mainshocks) are commonly
 64 assumed to follow a Poisson process with an underlying stationary rate (Ogata, 1988).
 65 The Omori law states that the occurrence rate of aftershocks follows as a power law de-
 66 cay with time (Utsu, 1961, 1972). The probability distribution of the (scalar) interevent
 67 times of successive earthquakes in a certain region has been found to satisfy a scaling
 68 function; it is well fitted by a general gamma distribution in real data (Bak et al., 2002;
 69 Corral, 2003, 2004) similar to that found later in rock fracture experiments in labora-
 70 tories (Davidsen et al., 2007). Some of the theoretical framework of the interevent times
 71 is based on the Gutenberg-Richter and the Omori laws (Saichev & Sornette, 2006; Sor-
 72 nette et al., 2008). Yet, there is some criticism regarding the universal scaling with the
 73 region size (Touati et al., 2009).

74 Another dominant feature of earthquakes is the clustering (memory) in space and
 75 time (Zaliapin et al., 2008; Zaliapin & Ben-Zion, 2013), generally at shorter time scales,
 76 including those for earthquake aftershock sequences and swarms. In addition, long-range
 77 memory in the time series of interevent times has been found using detrended fluctua-
 78 tion analysis (DFA) (Lennartz et al., 2008); strong memory was also found using the con-
 79 ditional probability of successive events (Livina et al., 2005). Some clustering models such
 80 as the Epidemic-Type Aftershock Sequence (ETAS) model (Ogata, 1998) and the short-
 81 term earthquake probability (STEP) model (Woessner et al., 2010) have been developed
 82 based on the short-term spatiotemporal clustering in earthquakes. In the ETAS model,
 83 the productivity parameter α is critical in controlling the short-term memory of interevent
 84 times (Fan et al., 2019). Furthermore, an extended analysis of both short and long-term
 85 memory of interevent times in real data and the ETAS model (Zhang et al., 2020) in-
 86 dicated that the inferred memory at all timescales cannot be captured by the ETAS model.
 87 A generalized (bimodal) ETAS model with two α -values was proposed to capture short-
 88 and long-term aftershock triggering mechanisms (Zhang et al., 2021); this model repro-
 89 duced the observed memory behavior in both short and long-time scales as found in real
 90 catalogs. This could be due to a sudden stress change in short-time scale and subsequent
 91 viscous relaxation in long-time scale.

92 The occurrence of aftershocks produces an obvious asymmetry in the time series,
 93 with more events after a previous one than before the next on the timescales of a sin-
 94 gular sequence. However, we may expect this asymmetry to degrade at longer timescales,
 95 where spontaneous events and the likelihood of overlapping aftershock sequences destroy-
 96 ing the correlation increases, as proposed by Touati et al. (2009). Asymmetry widely ex-
 97 ists in nature (An, 2004; Hutchinson et al., 2013) in time series for various geophysical
 98 phenomena including the glacial-interglacial cycles (rapid warming followed by gradual
 99 cooling), the sunspot cycle (11 years) (Hoyt & Schatten, 1998), and river flow which de-
 100 cays slowly and increases rapidly (Livina et al., 2003). In many cases, such asymmetry
 101 can be related to underlying non-equilibrium and nonlinear underlying processes in a phys-
 102 ical system (King, 1996; Schreiber & Schmitz, 1996). For instance, in the climate sys-
 103 tem, due to cyclone activity, surface daily mean temperature warms gradually and cools
 104 rapidly at the mid-latitudes leading to the temporal temperature asymmetry in the tem-
 105 perature time series (Ashkenazy et al., 2008). Here, we investigate asymmetry in earth-
 106 quake time series. For triggered events, the Omori law implies that the interevent time
 107 increases with time after a mainshock. Thus, one expects asymmetry in earthquake cat-
 108 alogs at short to intermediate time scales where there are not too many overlapping af-
 109 tershock sequences. For the spontaneous events, the interevent time is simply assumed
 110 to follow an exponential distribution with a constant rate, and asymmetry is not expected
 111 in this (Poisson process) case. In the following we show that the degree of asymmetry
 112 changes when considering the lagged interevent times.

2 Materials and Methods

2.1 Asymmetry

Based on earthquake catalogs, we consider seismic events above a certain magnitude threshold (i.e. the magnitude of completeness for the given catalogue). For this sequence, we define the time interval between two successive earthquake events $i+1$ and i as the interevent time τ_i (in days). The lagged interevent time increment is defined as $\Delta\tau_i^{(k)} = \tau_{i+k} - \tau_i$ for a lag k where k is a positive integer lag. Following the above, the asymmetry measure of interevent times is defined as the ratio between the number of positive interevent time increments, N_p , minus the number of negative increments, N_n , and the total (positive plus negative) increments (Ashkenazy et al., 2008):

$$U(k) = \frac{N_p - N_n}{N_p + N_n} = \frac{\sum_i \Theta(\tau_{i+k} - \tau_i) - \sum_i \Theta(\tau_i - \tau_{i+k})}{\sum_i \Theta(\tau_{i+k} - \tau_i) + \sum_i \Theta(\tau_i - \tau_{i+k})}, \quad (1)$$

where $\Theta(\tau) = 1$ when $\tau > 0$ and otherwise it is zero. We exclude the zero increments $\Delta\tau_i^{(k)} = 0$ from the calculation; the number of zero increments is indeed very small. U is bounded between -1 (monotonically decreasing sequence) and 1 (monotonically increasing sequence). When U is close to zero, the time series is symmetric (for example, the PDF is nearly symmetrical close to $\Delta\tau^{(k)} = 0$ for $k = 1$ but highly asymmetric for $k = 10$ and $k = 50$ in Figure 2(a)). For instance, if the asymmetry value of $U = 1/3$, the number of positive increments N_p is twice the number of negative increments N_n (i.e., $N_p = 2N_n$). The positive (negative) increment of the interevent time represents the decreasing (increasing) earthquake rate. Similarly, we define the asymmetry of the interevent distance r_i (in km) between the epicenters.

2.2 Generalized ETAS model

We also study the asymmetry of synthetic catalogs based on the ETAS model in comparison to the asymmetry observed in the time series of real records. We use the ETAS model as a null hypothesis, since it is the most widely used statistical model to simulate the spatiotemporal clustering of seismic events (Ogata, 1988, 1998). The earthquake sequence in the ETAS is defined as a stochastic Hawkes (point) process. We use the Gutenberg–Richter law (where $b = 1$, truncated at M_{max}) to independently generate the magnitude of each earthquake ($\geq M_0$). For the ETAS model, the conditional intensity function λ (which is basically the rate of earthquakes) at time t with the seismic history H_t prior to t is given by

$$\lambda(t|H_t) = \mu + \sum_{i:t_i < t} f(M_i, t - t_i), \quad (2)$$

where μ is the background rate to generate spontaneous earthquakes estimated from the real catalogs (Zhuang et al., 2010; Zhuang, 2012). The occurrence times of the past events are represented as t_i , and their magnitudes are M_i ($\geq M_0$). Future earthquakes can be triggered by each past earthquake according to the generalized triggering function which here includes two triggering processes (Zhang et al., 2021), as

$$f(M_i, t - t_i) = \begin{cases} \frac{Ac^p \exp[\alpha_1(m_i - M_0)]}{(t - t_i + c)^p} & i > n - n_c \\ \frac{Ac^p \exp[\alpha_2(m_i - M_0)]}{(t - t_i + c)^p} & i \leq n - n_c \end{cases}, \quad (3)$$

where $n - 1$ is the total number of past events. The productivity of triggering earthquakes is controlled by the two productivity parameters α_1 and α_2 corresponding to the short-term ($i > n - n_c$) and long-term ($i \leq n - n_c$) triggering respectively, which satisfy $\alpha_1 \geq \alpha_2$. If the interevent number $n - i$ is smaller than the crossover number n_c , the n -th earthquake can be triggered by the i -th historical earthquake with a higher rate according to the larger α_1 . The crossover number n_c is equal to $h10^{-bM_0}$ which is estimated from the memory measure of real earthquake catalog as reported by Zhang et al. (2021). Also, we use the parameters $\{A, c, p, h, \alpha_1, \alpha_2\}$ in Eq. (3) estimated from real

134 earthquake catalogs (Zhang et al., 2021). The generalized ETAS model reduces to the
 135 standard ETAS model if $\alpha_1 = \alpha_2$. We add only two parameters, α_2 and n_c to the stan-
 136 dard ETAS model and all other parameters remain the same. Note that when α_1 is dif-
 137 ferent with α_2 , Eq. 3 is a discontinuous function. Yet, it is very hard to observe a sys-
 138 tematical discontinuity in synthetic catalogs of the generalized ETAS model as well as
 139 real data, since the cascading triggering process of aftershocks can weaken the discon-
 140 tinuity (Zhang et al., 2021).

141 2.3 Data

142 We analyze the Italian earthquake catalog between 1981 and 2017 (Gasperini et
 143 al., 2013). We also analyzed the Japan Unified High-Resolution Relocated Catalog for
 144 Earthquakes (JUICE) between 2001 to 2012 (Yano et al., 2017) and the Southern Cal-
 145 ifornia catalog from 1981 to 2018 (Hauksson et al., 2012). The three catalogs are com-
 146 plete for magnitude threshold 3.0 (Hauksson et al., 2012; Gasperini et al., 2013; Yano
 147 et al., 2017) and this is also shown in Figure S1 where the distributions of the magni-
 148 tudes (≥ 3) follow the Gutenberg-Richter law.

149 3 Results

150 First, we obtain interevent times of the Italian earthquake catalog (using the thresh-
 151 old of magnitude $M_0 = 3.0$) and their increments for the lag index $k = 50$. The re-
 152 sults are shown in Fig. 1. As can be seen, interevent times decrease abruptly and then
 153 increase gradually after the occurrence of a large earthquake (Fig 1(a)), consistent with
 154 the Omori law. The increments are very small immediately after large shocks even for
 155 $k = 50$, and most of them are positive (see inset figure) in Fig. 1(b). After sufficient
 156 time from a main shock, a crossover time, the rate of aftershocks decreases and the in-
 157 terevent increments become symmetric and switch between negative and positive val-
 158 ues. Moreover, Fig. 1(b) shows that the interevent time increments for lag $k = 50$ tend
 159 to be negative before the occurrence of large earthquakes. This observation can be ex-
 160 plained as follows. The event time intervals before the main shock are relatively large
 161 in comparison to the event time intervals after the main shock, since the earthquake (af-
 162 tershock) rate after the main shock is high. The difference between time interval for lag
 163 $k = 50$, $\Delta\tau_i^{(k=50)}$, as approaching the main shock, involves the subtraction of a long-
 164 time interval before the main shock from a short time interval after the main shock, lead-
 165 ing to negative $\Delta\tau_i^{(k=50)}$. Thus, $\Delta\tau_i^{(k=50)}$ will be negative 50 lags preceding the main
 166 shock.

167 Fig. 2(a) shows the Probability Density Function (PDF) of the interevent time in-
 168 crements for different k . The PDFs are essentially asymmetric about $\Delta\tau^{(k)} = 0$ when
 169 k increases and the asymmetry is dominated by the points close to $\Delta\tau^{(k)} = 0$. To ver-
 170 ify the significance of the asymmetry, we randomly shuffled the time series of interevent
 171 times and produced 100 shuffled sequences. This shuffling procedure destroys the (tem-
 172 poral) aftershock clustering such that the number of positive and negative increments
 173 should be similar. As a result, the number of small increments decreases and the num-
 174 ber of large increments increases and the peak of the PDF (see gray shades in Fig. 2(a))
 175 is much lower than the peak of the PDF of the original catalog. For a larger increment
 176 lag of $k = 10, 50$, the PDF becomes more asymmetric in comparison to PDF with $k =$
 177 1 and the PDF of the shuffled data [Fig.2(a)]. More positive increments are observed for
 178 the larger lag-index k .

179 To quantify the level of the asymmetry, we calculate the measure U as a function
 180 of lag-index k using Eq. (1). Fig. 2(b) depicts, for the Italian catalog, the measure U
 181 for the interevent times (red) as a function of the lag increment k . The asymmetry mea-
 182 sure, U , increases with k for k below a crossover lag, $k_c \approx 50$, and decreases with k above
 183 the crossover k_c ; U is maximal at the crossover k_c until it is indistinguishable from the

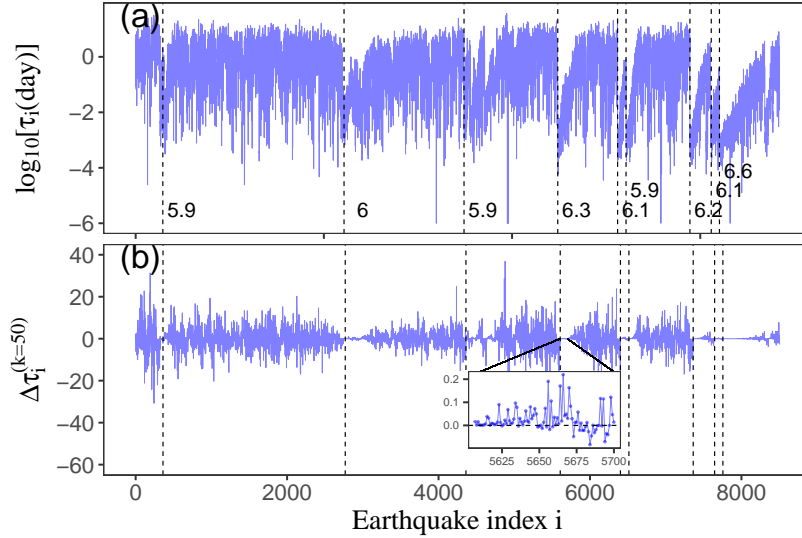


Figure 1. Time series of (a) interevent times (log scale) and (b) their increments for $k=50$ for the Italian catalog (1981–2017) using magnitude threshold 3.0. The inset figure shows the increments immediately after a large shock, indicating large asymmetry even for $k = 50$. The black dashed vertical lines show the large earthquakes (magnitudes ≥ 5.8). Note the episodes of very small $\Delta\tau^{(k=50)}$ after large earthquakes; yet, these occur during very short time and will hardly be visible when plotting $\Delta\tau^{(k=50)}$ versus time.

184 random process shown at high k . As discussed above, we expect the presence of asym-
 185 metry in the interevent times following the Omori-law [Fig. 1 and Fig. 2(a)]. Yet, the
 186 non-monotonic behavior with maximal asymmetry at k_c is not trivial which implies a
 187 transition between the effect of the Omori-law and a random process. We also calculated
 188 the asymmetry measure, U , for interevent distances (green symbols in Fig. 2(b)) and ob-
 189 served similar behavior as for the interevent times, although much less pronounced. The
 190 results of shuffled, symmetric, time series (gray shaded area) are also included in Fig.
 191 2(b) and indicate significant asymmetry for interevent times compared to this null hy-
 192 pothesis over a wide range of lags ($k < 300$). For interevent distances we observe weak
 193 asymmetry only around lag $k = 100$.

194 We also calculated the asymmetry measure, U , for three magnitude thresholds and
 195 three places. Fig. 3(a), (c) and (e) show U versus the index k for the interevent times
 196 when using different magnitude thresholds $M_0 = 3, 3.3$ and 3.6 for the catalogs of Italy
 197 (IT), Southern California (SC) and Japan (JA). The asymmetry measure, U , exhibits
 198 similar increasing and decreasing trends for all three catalogs. The crossover lag, k_c , (at
 199 which the asymmetry is maximal) is smaller for the larger magnitude threshold (see Fig.
 200 3(a), (c) and (e)). According to the Gutenberg-Richter law, the number of earthquakes
 201 decreases exponentially with the increasing magnitude threshold. Thus, we rescale the
 202 lag k with $k10^{bM_0}$ and the results are shown in Fig. 3(b), (d) and (f). The different asym-
 203 metry curves collapse into a single curve for which the crossover is $k_c10^{bM_0}$; this scal-
 204 ing approach is similar to the scaling procedure of interevent times discussed in previ-
 205 ous studies (Bak et al., 2002; Corral, 2003; Saichev & Sornette, 2006; Sornette et al., 2008).
 206 However, the crossovers are not the same for different places. For IT, the rescaled crossover
 207 lag is, $k_c10^{bM_0} \approx 5 \times 10^4$ and is smaller than the crossovers for JA ($k_c10^{bM_0} \approx 2 \times 10^5$)
 208 and SC ($k_c10^{bM_0} \approx 3 \times 10^5$). The asymmetry curves also satisfy the scaling relation
 209 by rescaling the lag k with the averaged time intervals $\langle\tau\rangle$ as shown in Fig. S2. We thus
 210 obtain that the crossover times approximately correspond to 80, 280, and 50 days for IT,

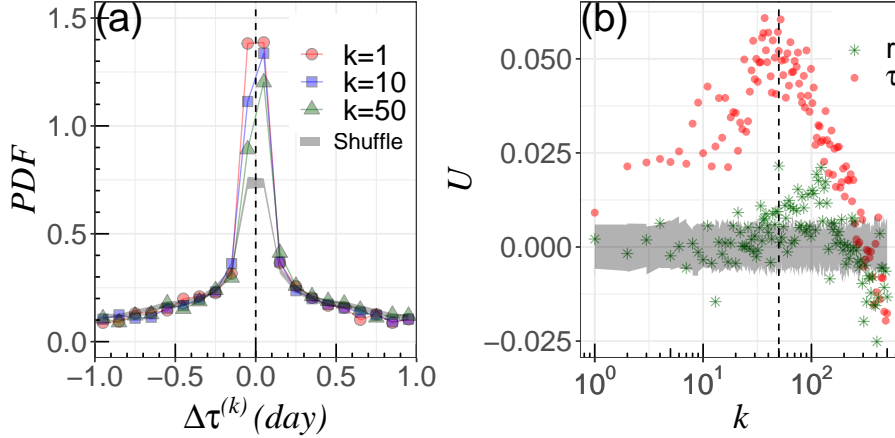


Figure 2. (Color online) (a) PDF of interevent time increments $\Delta\tau^{(k)}$ for different lag index k for the Italian catalog with the threshold $M_0 = 3.0$. (b) The asymmetry measure U versus the index k for the interevent times (red) τ and distances (green) r for the Italian catalog with $M_0 = 3.0$. Gray shades show the results of the shuffled (randomized) interevent times and distances and their standard deviations; these overlap each other. The dashed black line in (b) indicates the crossover lag $k_c \approx 50$ at which the asymmetry measure U for interevent times is maximal.

211 SC and JA respectively. We also consider and observed the asymmetry for different re-
 212 gion sizes as shown in Fig. S3(a). A smaller region size shows a larger asymmetry since
 213 more events (aftershocks) are correlated within the area as proposed by Touati et al. (2009).
 214 Moreover, the crossover can be scaled with respect to region size in Fig. S3(b). Figure
 215 S4 shows the weak asymmetry for the global earthquake catalog.

216 We now aim to explain the mechanism underlying the observed asymmetry measure-
 217 sure. Considering a simple situation, for which aftershocks $B-F$ are the first generation
 218 aftershocks triggered by a mainshock A , as shown by the schematic drawing in Fig. 4(a).
 219 Due to the Omori law, the frequency of aftershocks decreases like $(t-t_0)^{-p}$ (p is close
 220 to 1 and $t-t_0$ is the time since the mainshock) such that the interevent time τ after
 221 the mainshock follows $\tau \sim (t-t_0)^p$. Thus, the interevent time statistically increases
 222 with time, resulting in a positive asymmetry with more positive increments in compar-
 223 ison to negative increments. However, the real situation is more complex as not only main-
 224 shocks can trigger aftershocks but aftershocks can also trigger other aftershocks. More-
 225 over, spontaneous earthquakes (mainshocks) could be mixed with aftershocks due to the
 226 stacking involved (see the example in Fig. 4(b)). The indirect triggered events and the
 227 spontaneous events can decrease the interevent times as shown in Fig. 4(b) (τ_2, τ_3 and
 228 τ_5 are smaller than τ_1). The above considerations implies that the events below the crossover
 229 lag k_c are mainly triggered by a mainshock. Above the crossover ($k > k_c$), the sequences
 230 for spontaneous and triggered events will overlap with high probabilities resulting in a
 231 fast decay of asymmetry.

232 The ETAS model is widely used to simulate and study the temporal clustering of
 233 seismic events (Ogata, 1988, 1998). The rate function of the ETAS model consists of the
 234 spontaneous (background) rate and triggering rate of historical events (see Eq. (2)). The
 235 choice of parameters in the ETAS model is critical to reproduce the features of real earth-
 236 quake sequences. The maximum likelihood estimation (MLE) procedure has been pro-
 237 posed (Zhuang et al., 2010) to estimate the parameters. In a recent study (Zhang et al.,
 238 2021) the conventional ETAS model has been found to be unable to reproduce impor-

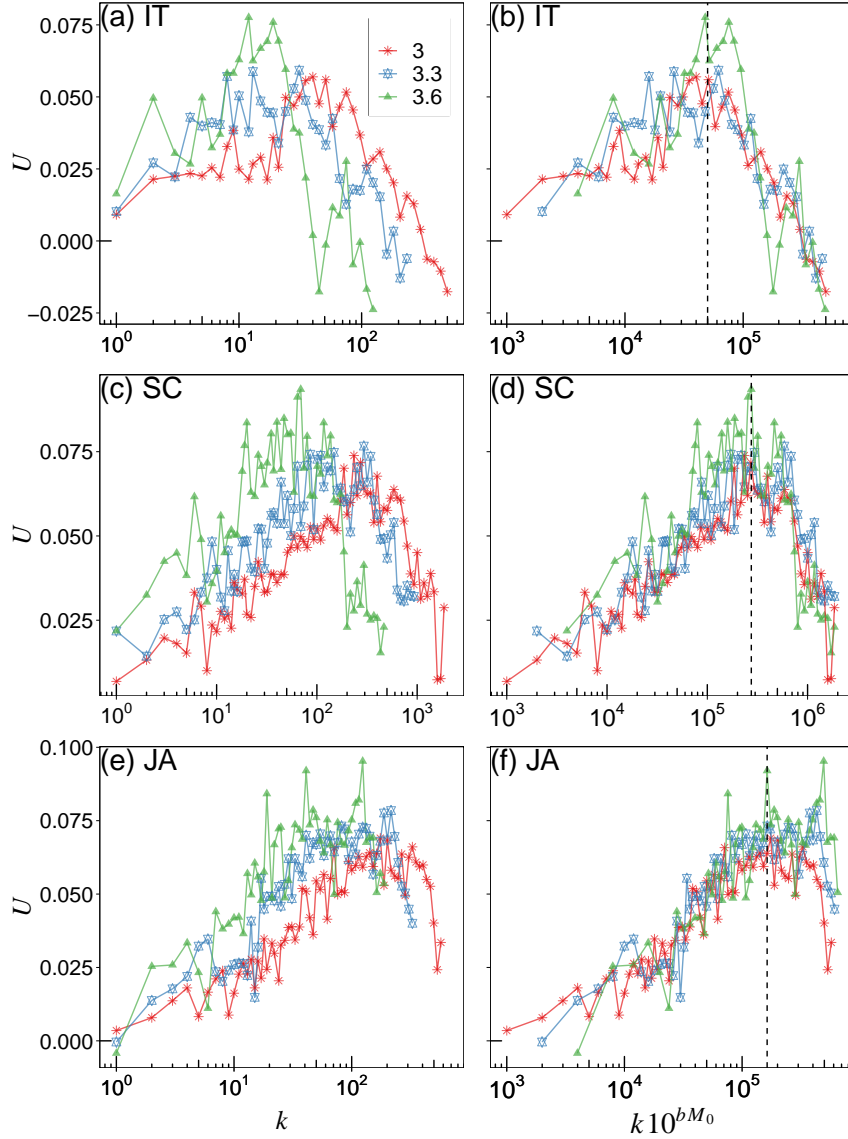


Figure 3. (Color online) The asymmetry measure U versus the index k for the interevent times with different magnitude thresholds $M_0 = 3, 3.3$ and 3.6 for the earthquake catalogs of (a) Italy (IT), (c) Southern California (SC) and (e) Japan (JA). (b), (d) and (f) Same as (a), (c) and (e) but x -axis is rescaled as $k10^{bM_0}$. Dashed black lines indicate the approximate crossover lag.

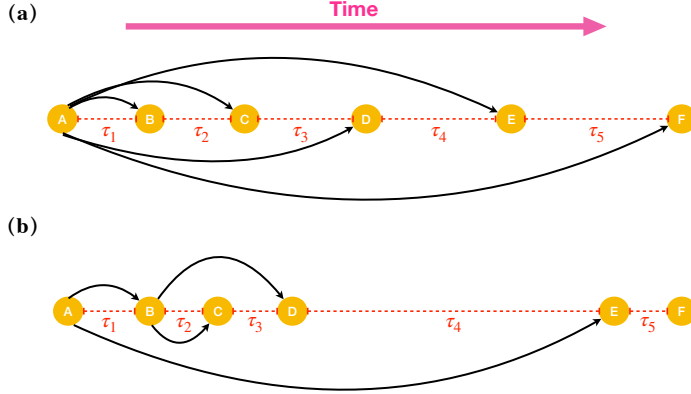


Figure 4. Cartoon illustrating how interevent times in earthquakes change with time for (a) the aftershocks B – F directly triggered by A (mainshock), and (b) the first generation of aftershocks B , and E triggered by A , the second generation of aftershocks C , and D triggered by B and the spontaneous event F . Dashed red lines represent interevent times.

Table 1. Estimated parameters of the three versions of the ETAS model for the Italian catalog. The parameters of EM0 are taken from (Lombardi, 2015) which have been estimated by MLE. For EM1, the parameters α_1 , α_2 are larger than EM0, and A is smaller, to guarantee similar earthquake rate as the real catalog. We select the parameters of EM2 based on recent findings (Zhang et al., 2021).

	μ	c	p	A	α_1	α_2	h
EM0	0.2	0.007	1.13	6.26	1.4	1.4	–
EM1	0.2	0.007	1.13	2.91	2.0	2.0	–
EM2	0.2	0.007	1.13	3.35	2.0	1.4	2×10^5

239 tant (long-term) memory characteristics observed in real catalogs. In the same study a
 240 generalized the ETAS model has been developed and found to be useful in reproducing
 241 the observe memory features that appear in the real catalogs (see Materials and Meth-
 242 ods). Below we test the asymmetry of the generalized ETAS model for Italy with three
 243 choices of parameters: (I) $\alpha_1 = \alpha_2 = \alpha$ such that the generalized model reduces to
 244 the standard ETAS model. The parameters are estimated using the MLE. This choice
 245 is termed “EM0”. (II) Since some studies have reported that the α -value is underesti-
 246 mated by the MLE (Marzocchi & Lombardi, 2009; Seif et al., 2017; Zhuang et al., 2019),
 247 we consider a second choice of parameters termed “EM1”, which is the same as EM0 but
 248 with larger α (and smaller A to guarantee the similar branching ratio) (Eq. (3)). (III)
 249 The generalized ETAS model with $\alpha_1 > \alpha_2$ developed recently (Zhang et al., 2021). This
 250 choice is termed “EM2”. The selected parameters of EM0, EM1 and EM2 for the Ital-
 251 ian catalog are listed in Table 1. We generated 50 realizations of synthetic catalogs with
 252 magnitudes greater than or equal to magnitude 3, each covering 50000 days. The earth-
 253 quake rates are 0.69 ± 0.03 , 0.73 ± 0.1 and 0.71 ± 0.06 events per day for EM0, EM1 and
 254 EM2 respectively. The rates of the models are similar and close to that of the real data.

255 Next, we study the asymmetry for the three versions of the ETAS model introduced
 256 above. Figure 5(a) shows that the asymmetry of the interevent times in the standard
 257 ETAS, EM0, in marked contrast with real asymmetry, decreases with the lag index k with-

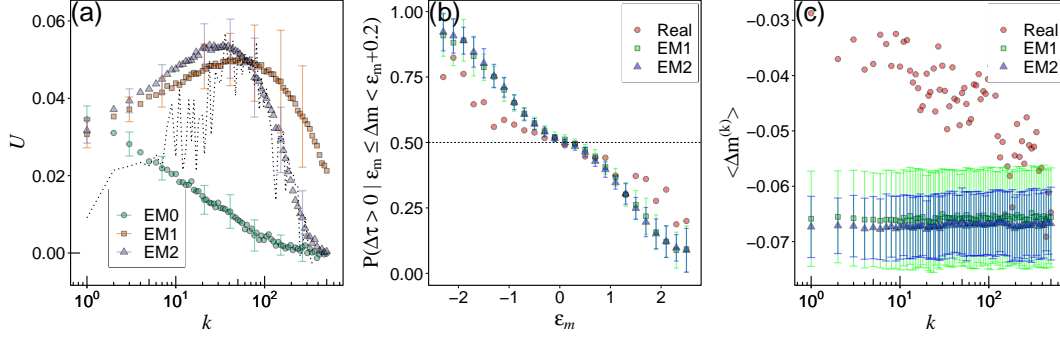


Figure 5. (color online) (a) The asymmetry measure U versus the index k for the interevent times of the synthetic Italian catalogs using EM0, EM1 and EM2 with magnitude threshold 3. The asymmetry of the real Italian catalog is indicated by the dotted line. (b) Conditional probability $P(\Delta\tau > 0 | \epsilon_m \leq \Delta m < \epsilon_m + 0.2)$ as a function of the magnitude increment ϵ_m for the real Italian catalog and synthetic catalogs of EM1, EM2. (c) The average of the magnitude increment $\langle \Delta m^{(k)} \rangle$ for $\tau_i < 0.5$ days versus the index k . The measures and their error bars are calculated based on the means and the standard deviations of 50 independent realizations for the models.

258 out a crossover for EM0 (green dots). Both, EM1 (red squares) and EM2 (green trian-
 259 gles) exhibit much better performance and their asymmetry curves are similar to the
 260 real catalog (dotted line). Due to the smaller α in EM0 relative to EM1, the probability of
 261 aftershocks directly triggered by a large mainshock is too low to increase the asymme-
 262 try for EM0. Thus, the asymmetry decreases as the lag index k increases at the begin-
 263 ning rather than after a certain lag. The asymmetry of EM0 demonstrates that the α -
 264 value is indeed underestimated by MLE. Comparing between EM1 and EM2, the asym-
 265 metry of EM2 decays faster above the crossover, more similar to the decay of the real
 266 catalog, the dotted line (see Fig. 5(a)). Moreover, the crossover point is different for EM1
 267 ($k_c \approx 60$) and EM2 ($k_c \approx 50$). Thus, the crossover of EM2 is closer to the observed
 268 one (Fig. 5(a)). We thus conclude that the two-alpha ($\alpha_1 > \alpha_2$) ETAS model exhibits
 269 the best performance in reproducing both the memory (Zhang et al., 2021) and asym-
 270 metry in the current study than both versions of the standard ETAS model. The asym-
 271 metry of EM2 also satisfies the scaling relation for the magnitude threshold similar to
 272 the real one (see SI, Figure S5).

273 We further study the dependence of the interevent time increments $\Delta\tau_i^k$ on the mag-
 274 nitude increment $\Delta m_i^{(k)} = m_{i+k} - m_i$, to understand in more details the role of Omori
 275 law on the asymmetry. For this purpose we calculated the conditional probability $P(\Delta\tau >$
 276 $0 | \epsilon_m \leq \Delta m < \epsilon_m + d)$, where $d = 0.2$ is the bin size of the magnitude increment. Fig-
 277 ure 5(b) shows that this conditional probability decreases when the magnitude increment
 278 ϵ_m increases, for the real, EM1 and EM2 catalogs;. Moreover, the conditional probab-
 279 ility is around 0.5 (corresponding to the asymmetry measure around zero) when ϵ_m is close
 280 to zero. Thus, the asymmetry measure close to zero could be due to the magnitude sim-
 281 ilarity for small lag-index k , as the PDF interevent time increments is maximal close to
 282 zero (Fig 2(a)). Previous studies (Lippiello et al., 2008, 2012) have found that the mag-
 283 nitude of consecutive events is more similar than would be expected from random sam-
 284 pling of the Gutenberg-Richter distribution. It is apparent that EM1 and EM2 overes-
 285 timate the conditional probability of the real data. Fig. 5(c) shows the average of the
 286 magnitude increment $\langle \Delta m^{(k)} \rangle$ for $\tau_i < 0.5$ days (to focus on aftershocks) as a func-
 287 tion of the lag-index k . The size of aftershock is usually smaller than the mainshock yield-
 288 ing the negative values in Figure 5(c). Yet, it is also clear that while the mean magni-
 289 tude difference $\langle \Delta m^{(k)} \rangle$ is almost constant with lag k for EM1 and EM2, it decreases

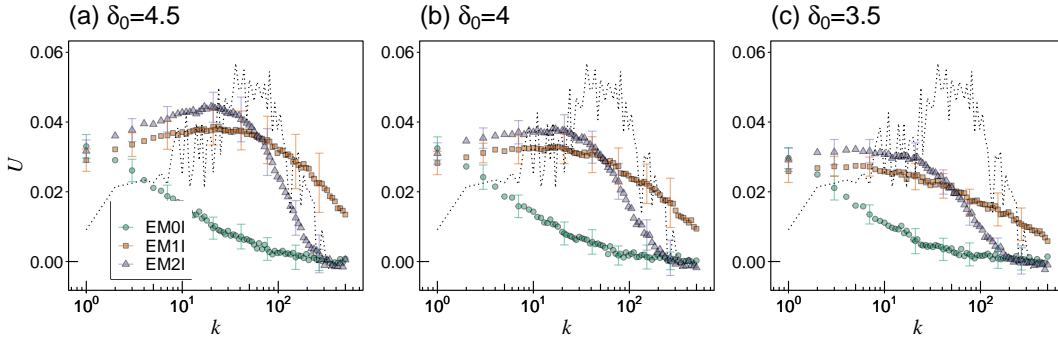


Figure 6. (Color online) The asymmetry measure U versus the index k for the interevent times of the synthetic incomplete catalogs using EM0I, EM1I and EM2I with magnitude threshold 3 for (a) $\delta_0 = 4.5$ (EM0I with $\alpha_1 = \alpha_2 = 1.41$, EM1I with $\alpha_1 = \alpha_2 = 2.01$, and EM2I with $\alpha_1 = 2.01$ and $\alpha_2 = 1.40$), (b) $\delta_0 = 4.0$ (EM0I with $\alpha_1 = \alpha_2 = 1.42$, EM1I with $\alpha_1 = \alpha_2 = 2.02$, and EM2I with $\alpha_1 = 2.02$ and $\alpha_2 = 1.40$) and (c) $\delta_0 = 3.5$ (EM0I with $\alpha_1 = \alpha_2 = 1.44$, EM1I with $\alpha_1 = \alpha_2 = 2.04$, and EM2I with $\alpha_1 = 2.04$ and $\alpha_2 = 1.40$). The asymmetry of the real Italian catalog is indicated by the dotted line.

290
291
292

for the real catalog, from values closer to zero for small lag-index k to values of EM1 and EM2 at large k (Fig. 5(c)). These results indicate that the magnitude similarity reported by (Lippiello et al., 2008, 2012) is absent in both models.

While the asymmetry of EM2 is similar to the asymmetry of the real catalog for $k > 300$, it is significantly higher for smaller k (Fig. 5(a)). The Italian catalog we used has been reported to be complete above magnitude threshold 3.0. (Gasperini et al., 2013). However, due to the inefficiency of the seismic network and the overlapping of aftershock seismograms, an earthquake catalog could be incomplete, especially after mainshocks (Kagan, 2004; Hainzl, 2016; de Arcangelis et al., 2018). To investigate the effect of the incompleteness of the catalogs, we generate synthetic incomplete catalogs based on the studies of Helmstetter et al. (2006); Seif et al. (2017); Petrillo and Lippiello (2021). The incomplete ETAS model is based on the conditional earthquake rate intensity function as (Petrillo & Lippiello, 2021),

$$\lambda_I(m, t) = \lambda \times \prod_i \Phi(m|M_i(t-t_i), \sigma), \quad (4)$$

where all past events with $t_i < t$ are considered. We define $\Phi(m|M_i(t-t_i), \sigma) = 1$ when $m > M_i(t-t_i) + \sigma$, $\Phi(m|M_i(t-t_i), \sigma) = 0$ when $m < M_i(t-t_i) - \sigma$, $\Phi(m|M_i(t-t_i), \sigma) = 0.5$ else. The magnitude threshold $M_i(t-t_i)$ is calculated as (Kagan, 2004; Hainzl, 2016; de Arcangelis et al., 2018),

$$M_i(t-t_i) = m_i - \delta_0 - \omega \log_{10}(t-t_i), \quad (5)$$

293
294
295
296
297

where m_i is the magnitude of past event i , and $t-t_i$ is the time since the past event. The parameter $\sigma = 0.6$ is chosen following Petrillo and Lippiello (2021) and Seif et al. (2017); Helmstetter et al. (2006) suggested the following parameter values $\delta_0 = 4.5$ and $\omega = 0.75$. We consider three different choices of the parameter δ_0 , $\delta_0 = 4.5, 4.0$, and 3.5 to generate synthetic catalogs with different degree of incompleteness.

298
299
300
301

To generate the synthetic incomplete catalogs based on EM0, EM1 and EM2 (represented as EM0I, EM1I and EM2I respectively), we remove an aftershock i from the synthetic complete catalogs with a probability given by $\prod_i \Phi(m|M_i(t-t_i), \sigma)$ (Petrillo & Lippiello, 2021). To roughly preserve the total number of earthquakes to be the same

302 as that of Figure 5(a), we increased slightly the α parameter and left the other param-
 303 eters unchanged. With this procedure, the level of incompleteness of each synthetic cat-
 304 alog was 5%, 10% and 20% for $\delta_0 = 4.5$, 4.0, and 3.5 respectively for EM1I and EM2I;
 305 the percentages indicate the relative number of events that has been removed from the
 306 complete catalog. It is apparent from our results (see Figure 6) that the asymmetry weak-
 307 ens as the degree of incompleteness is higher. Still, for both models, the asymmetry is
 308 overestimated for small lag index k in comparison to the real catalog and weakens when
 309 the catalogs are more incomplete. Figure S6 shows similar results when using $\sigma = 0.6$,
 310 1.2, 1.8 to control the degree of incompleteness. We also try to control the parameter
 311 A to keep the same number of earthquakes for EM0I, EM1I and EM2I and the results
 312 are shown in Figure S7.

313 4 Conclusions

314 Here, we investigated the asymmetry behavior of interevent times (and distances)
 315 in earthquake catalogs. For real seismic catalogs, the asymmetry as a function of k first
 316 increases up to a crossover lag k_c and then decreases rapidly. The crossover lag k_c changes
 317 with location and with the magnitude threshold, where the latter can be rescaled to uni-
 318 fied value of $k_c 10^{bM_0}$. We suggest that the Omori law is associated with the increase of
 319 the asymmetry below the crossover and has a decreasing influence above this crossover.
 320 This is probably due to the overlapping of different triggered aftershocks and the spon-
 321 taneous events that lead to a fast decay of asymmetry above the crossover. The de-clustering
 322 between spontaneous and triggered earthquake events is still an open important ques-
 323 tion (Zaliapin et al., 2008; Zaliapin & Ben-Zion, 2013). The asymmetry results reported
 324 here and its associated crossover may help to resolve this question although this requires
 325 further investigation.

326 In the standard ETAS model whose parameters are estimated by MLE, the increase
 327 of asymmetry and the crossover cannot be reproduced. When the α -value is increased,
 328 a large mainshock can trigger more aftershocks such that there exists an increasing trend
 329 and a crossover in the standard ETAS model. This demonstrates that the common α -
 330 value is indeed underestimated by MLE. However, the crossover value of k is larger and
 331 the asymmetry above the crossover is significantly higher and decays slower in the stan-
 332 dard ETAS model with large α than the real one. The generalized ETAS model with two
 333 α -values ($\alpha_1 > \alpha_2$) in short and long time scales exhibits similar asymmetry behavior
 334 as that of the real catalog for lags larger than the crossover lag k_c . Yet, the asymmetry
 335 for small lag-index k is overestimated by both models (one and two α -value). We sug-
 336 gest that the short-term symmetrical behavior can be attributed to the magnitude simi-
 337 larity in real data which is missing in both models. The additional advantage of the gen-
 338 eralized ETAS model is its ability to reproduce the observe memory in earthquake cat-
 339 alogs as reported in (Zhang et al., 2021). Thus, generally speaking, the asymmetry find-
 340 ings reported here may be used to improve earthquake forecasting models as the asym-
 341 metry measure can serve as an additional characteristic that a forecasting model should
 342 reproduce.

343 Acknowledgments

344 We thank for the financial support by the EU H2020 project RISE, the Israel Science
 345 Foundation (Grants No. 189/19), DTRA ,the Pazy Foundation, the joint China-Israel
 346 Science Foundation (Grants No. 3132/19) and the BIU Center for Research in Applied
 347 Cryptography and Cyber Security. We thank the Israel ministry of energy. We down-
 348 loaded the Southern California catalog from the SCEDC ([https://scedc.caltech.edu/research-
 349 tools/alt-2011-dd-hauksson-yang-shearer.html](https://scedc.caltech.edu/research-tools/alt-2011-dd-hauksson-yang-shearer.html)) (Hauksson et al., 2012) and the Japanese
 350 Catalog (JUICE) from ref (Yano et al., 2017). The Italian catalog is available on request
 351 from ref (Gasparini et al., 2013) and the authors.

References

352

- 353 An, S. I. (2004). Interdecadal changes in the El Nino-La Nina asymmetry. *Geophys.*
 354 *Res. Lett.*, *31*(23), 1–4. doi: 10.1029/2004GL021699
- 355 Ashkenazy, Y., Feliks, Y., Gildor, H., & Tziperman, E. (2008). Asymmetry
 356 of daily temperature records. *J. Atmos. Sci.*, *65*(10), 3327–3336. doi:
 357 10.1175/2008JAS2662.1
- 358 Bak, P., Christensen, K., Danon, L., & Scanlon, T. (2002). Unified Scaling Law for
 359 Earthquakes. *Phys. Rev. Lett.*, *88*(17), 178501. doi: 10.1103/PhysRevLett.88
 360 .178501
- 361 Corral, Á. (2003). Local distributions and rate fluctuations in a unified scaling law
 362 for earthquakes. *Phys. Rev. E*, *68*(3), 035102. doi: 10.1103/PhysRevE.68
 363 .035102
- 364 Corral, Á. (2004). Long-Term Clustering, Scaling, and Universality in the Tempo-
 365 ral Occurrence of Earthquakes. *Phys. Rev. Lett.*, *92*(10), 108501. doi: 10.1103/
 366 PhysRevLett.92.108501
- 367 Davidsen, J., Stanchits, S., & Dresen, G. (2007). Scaling and universality in rock
 368 fracture. *Phys. Rev. Lett.*, *98*(12), 125502. doi: 10.1103/PhysRevLett.98
 369 .125502
- 370 de Arcangelis, L., Godano, C., Grasso, J. R., & Lippiello, E. (2016). Statistical
 371 physics approach to earthquake occurrence and forecasting. *Phys. Rep.*, *628*,
 372 1–91. doi: 10.1016/j.physrep.2016.03.002
- 373 de Arcangelis, L., Godano, C., & Lippiello, E. (2018). The Overlap of Aftershock
 374 Coda Waves and Short-Term Postseismic Forecasting. *J. Geophys. Res. Solid*
 375 *Earth*, *123*(7), 5661–5674. doi: 10.1029/2018JB015518
- 376 Fan, J., Zhou, D., Shekhtman, L. M., Shapira, A., Hofstetter, R., Marzocchi, W., ...
 377 Havlin, S. (2019). Possible origin of memory in earthquakes: Real catalogs and
 378 an epidemic-type aftershock sequence model. *Phys. Rev. E*, *99*(4), 042210. doi:
 379 10.1103/PhysRevE.99.042210
- 380 Gasperini, P., Lolli, B., & Vannucci, G. (2013). Empirical calibration of local mag-
 381 nitude data sets versus moment magnitude in Italy. *Bull. Seismol. Soc. Am.*,
 382 *103*(4), 2227–2246. doi: 10.1785/0120120356
- 383 Gutenberg, B., & Richter, C. F. (1944). Frequency of Earthquakes in California.
 384 *Bull. Seismol. Soc. Am.*, *34*(4), 185–188. doi: 10.1038/156371a0
- 385 Hainzl, S. (2016). Rate-Dependent Incompleteness of Earthquake Catalogs. *Seismol.*
 386 *Res. Lett.*, *87*(2A), 337–344. doi: 10.1785/0220150211
- 387 Hauksson, E., Yang, W., & Shearer, P. M. (2012). Waveform Relocated Earthquake
 388 Catalog for Southern California (1981 to June 2011). *Bull. Seismol. Soc. Am.*,
 389 *102*(5), 2239–2244. doi: 10.1785/0120120010
- 390 Helmstetter, A., Kagan, Y. Y., & Jackson, D. D. (2006). Comparison of short-term
 391 and time-independent earthquake forecast models for southern california. *Bull.*
 392 *Seismol. Soc. Am.*, *96*(1), 90–106.
- 393 Hoyt, D. V., & Schatten, K. H. (1998). Group sunspot numbers: A new solar activ-
 394 ity reconstruction. *Sol. Phys.*, *179*(1), 189–219.
- 395 Huc, M., & Main, I. G. (2003). Anomalous stress diffusion in earthquake triggering:
 396 Correlation length, time dependence, and directionality. *J. Geophys. Res. Solid*
 397 *Earth*, *108*(B7). doi: 10.1029/2001jb001645
- 398 Hutchinson, D. K., England, M. H., Santoso, A., & Hogg, A. M. C. (2013). In-
 399 terhemispheric asymmetry in transient global warming: The role of Drake
 400 Passage. *Geophys. Res. Lett.*, *40*(8), 1587–1593. doi: 10.1002/grl.50341
- 401 Ide, S. (2013). The proportionality between relative plate velocity and seismicity in
 402 subduction zones. *Nat. Geosci.*, *6*(9), 780–784. doi: 10.1038/ngeo1901
- 403 Jordan, T. H., Chen, Y.-T., Gasparini, P., Madariaga, R., Main, I., Marzocchi, W.,
 404 ... Zschau, J. (2011). Operational earthquake forecasting. state of knowledge
 405 and guidelines for utilization. *Ann. Geophys.*, *54*(4), 361–391.

- 406 Kagan, Y. Y. (2004). Short-term properties of earthquake catalogs and models of
 407 earthquake source. *Bull. Seismol. Soc. Am.*, *94*(4), 1207–1228. doi: 10.1785/
 408 012003098
- 409 King, T. (1996). Quantifying nonlinearity and geometry in time series of climate.
 410 *Quat. Sci. Rev.*, *15*(4), 247–266. doi: 10.1016/0277-3791(95)00060-7
- 411 Lennartz, S., Livina, V. N., Bunde, A., & Havlin, S. (2008). Long-term memory
 412 in earthquakes and the distribution of interoccurrence times. *EPL*, *81*(6), 3–7.
 413 doi: 10.1209/0295-5075/81/69001
- 414 Lippiello, E., De Arcangelis, L., & Godano, C. (2008). Influence of time and space
 415 correlations on earthquake magnitude. *Phys. Rev. Lett.*, *100*(3), 1–4. doi: 10
 416 .1103/PhysRevLett.100.038501
- 417 Lippiello, E., De Arcangelis, L., & Godano, C. (2009). Role of static stress diffusion
 418 in the spatiotemporal organization of aftershocks. *Phys. Rev. Lett.*, *103*(3).
 419 doi: 10.1103/PhysRevLett.103.038501
- 420 Lippiello, E., Godano, C., & De Arcangelis, L. (2012). The earthquake magnitude
 421 is influenced by previous seismicity. *Geophys. Res. Lett.*, *39*(5). doi: 10.1029/
 422 2012GL051083
- 423 Livina, V. N., Ashkenazy, Y., Braun, P., Monetti, R., Bunde, A., & Havlin, S.
 424 (2003). Nonlinear volatility of river flux fluctuations. *Phys. Rev. E*, *67*(4),
 425 4. doi: 10.1103/PhysRevE.67.042101
- 426 Livina, V. N., Havlin, S., & Bunde, A. (2005). Memory in the Occurrence of Earth-
 427 quakes. *Phys. Rev. Lett.*, *95*(20), 208501. doi: 10.1103/PhysRevLett.95
 428 .208501
- 429 Lombardi, A. M. (2015). Estimation of the parameters of ETAS models by Simu-
 430 lated Annealing. *Sci. Rep.*, *5*(1), 8417. doi: 10.1038/srep08417
- 431 Marsan, D., & Lengliné, O. (2008). Extending earthquakes’ reach through cascading.
 432 *Science*, *319*(5866), 1076–1079. doi: 10.1126/science.1148783
- 433 Marzocchi, W., & Lombardi, A. M. (2009). Real-time forecasting following a damag-
 434 ing earthquake. *Geophys. Res. Lett.*, *36*(21). doi: 10.1029/2009GL040233
- 435 Ogata, Y. (1988). Statistical Models for Earthquake Occurrences and Residual Anal-
 436 ysis for Point Processes. *J. Am. Stat. Assoc.*, *83*(401), 9–27. doi: 10.1080/
 437 01621459.1988.10478560
- 438 Ogata, Y. (1998). Space-Time Point-Process Models for Earthquake Occurrences.
 439 *Ann. Inst. Stat. Math.*, *50*(2), 379–402. doi: 10.1023/A:1003403601725
- 440 Petrillo, G., & Lippiello, E. (2021). Testing of the foreshock hypothesis within an
 441 epidemic like description of seismicity. *Geophys. J. Int.*, *225*(2), 1236–1257.
- 442 Richards-Dinger, K., Stein, R. S., & Toda, S. (2010). Decay of aftershock den-
 443 sity with distance does not indicate triggering by dynamic stress. *Nature*,
 444 *467*(7315), 583–586. doi: 10.1038/nature09402
- 445 Saichev, A., & Sornette, D. (2006). “Universal” Distribution of Interearthquake
 446 Times Explained. *Phys. Rev. Lett.*, *97*(7), 078501. doi: 10.1103/PhysRevLett
 447 .97.078501
- 448 Schreiber, T., & Schmitz, A. (1996). Improved surrogate data for nonlinearity tests.
 449 *Phys. Rev. Lett.*, *77*(4), 635–638. doi: 10.1103/PhysRevLett.77.635
- 450 Seif, S., Mignan, A., Zechar, J. D., Werner, M. J., & Wiemer, S. (2017). Estim-
 451 ating ETAS: The effects of truncation, missing data, and model assumptions. *J.*
 452 *Geophys. Res. Solid Earth*, *122*(1), 449–469. doi: 10.1002/2016JB012809
- 453 Sornette, D., Utkin, S., & Saichev, A. (2008). Solution of the nonlinear theory and
 454 tests of earthquake recurrence times. *Phys. Rev. E*, *77*(6), 1–10. doi: 10.1103/
 455 PhysRevE.77.066109
- 456 Touati, S., Naylor, M., & Main, I. G. (2009). Origin and Nonuniversality of the
 457 Earthquake Intervent Time Distribution. *Phys. Rev. Lett.*, *102*(16), 168501.
 458 doi: 10.1103/PhysRevLett.102.168501
- 459 Utsu, T. (1961). A statistical study on the occurrence of af- tershocks. *Geophys.*
 460 *Mag.*, *30*, 521–605.

- 461 Utsu, T. (1972). Aftershocks and Earthquake Statistics (3) : Analyses of the
 462 Distribution of Earthquakes in Magnitude, Time and Space with Special Con-
 463 sideration to Clustering Characteristics of Earthquake Occurrence(1). *J. Fac.*
 464 *Sci. Hokkaido Univ. Ser. 7, Geophys.*, 4(1), 1–42.
- 465 Woessner, J., Christophersen, A., Douglas Zechar, J., & Monelli, D. (2010). Building
 466 self-consistent, short-term earthquake probability (STEP) models: Improved
 467 strategies and calibration procedures. *Ann. Geophys.*, 53(3), 141–154. doi:
 468 10.4401/ag-4812
- 469 Yano, T. E., Takeda, T., Matsubara, M., & Shiomi, K. (2017). Japan unified
 470 high-resolution relocated catalog for earthquakes (JUICE): Crustal seis-
 471 micity beneath the Japanese Islands. *Tectonophysics*, 702, 19–28. doi:
 472 10.1016/j.tecto.2017.02.017
- 473 Zaliapin, I., & Ben-Zion, Y. (2013). Earthquake clusters in southern California I:
 474 Identification and stability. *J. Geophys. Res. Solid Earth*, 118(6), 2847–2864.
 475 doi: 10.1002/jgrb.50179
- 476 Zaliapin, I., Gabrielov, A., Keilis-Borok, V., & Wong, H. (2008). Clustering analysis
 477 of seismicity and aftershock identification. *Phys. Rev. Lett.*, 101(1), 4–7. doi:
 478 10.1103/PhysRevLett.101.018501
- 479 Zhang, Y., Fan, J., Marzocchi, W., Shapira, A., Hofstetter, R., Havlin, S., & Ashke-
 480 nazy, Y. (2020). Scaling laws in earthquake memory for interevent times and
 481 distances. *Phys. Rev. Res.*, 2(1), 013264. doi: 10.1103/PhysRevResearch.2
 482 .013264
- 483 Zhang, Y., Zhou, D., Fan, J., Marzocchi, W., Ashkenazy, Y., & Havlin, S. (2021).
 484 Improved earthquake aftershocks forecasting model based on long-term mem-
 485 ory. *New J. Phys*, 23, 042001. doi: 10.1088/1367-2630/abeb46
- 486 Zhuang, J. (2012). Long-term earthquake forecasts based on the epidemic-type after-
 487 shock sequence (ETAS) model for short-term clustering. *Res. Geophys.*, 2(1),
 488 8. doi: 10.4081/rg.2012.e8
- 489 Zhuang, J., Murru, M., Falcone, G., & Guo, Y. (2019). An extensive study of
 490 clustering features of seismicity in Italy from 2005 to 2016. *Geophys. J. Int.*,
 491 216(1), 302–318. doi: 10.1093/gji/ggy428
- 492 Zhuang, J., Werner, M. J., Harte, D., Hainzl, S., & Zhou, S. (2010). Basic models of
 493 seismicity. *Community Online Resour. Stat. Seism. Anal.*, 2–41. doi: 10.5078/
 494 corssa-47845067.